Haptic fMRI : Accurately Estimating Neural Responses in Motor, Pre-Motor, and Somatosensory Cortex During Complex Motor Tasks

Samir Menon[1], Michelle Yu[1], Kendrick Kay[2], and Oussama Khatib[1]

Abstract—**Haptics combined with functional magnetic resonance imaging (Haptic fMRI) can non-invasively study how the human brain coordinates movement during complex manipulation tasks, yet avoiding associated fMRI artifacts remains a challenge. Here, we demonstrate confound-free neural activation measurements using Haptic fMRI for an unconstrained three degree-of-freedom motor task that involves planning, reaching, and visually guided trajectory tracking. Our haptic interface tracked subjects' hand motions, velocities, and accelerations (sample-rate, 350Hz), and provided continuous real-time visual feedback. During fMRI acquisition, we achieved uniform response latencies (reaching, 0.7–1.1s; tracking, 0.4–0.65s); minimized hand jitter (<8mm); and ensured reliable motion trajectories (tracking, <7mm root-mean-square error). In addition, our protocol decorrelated head motion from both hand speed (r=-0.03) and acceleration (r=-0.025), which reliably produced low head motion levels (<0.4mm/s between scan volumes) and a low fMRI temporal noise-to-signal ratio (<1%) across thirty-five scan runs. Our results address the primary outstanding Haptic fMRI confounds: motion induced low spatial-frequency magnetic field changes, which correlate neural activation across cortex; unreliable motions and response latencies, which reduce statistical power; and task-correlated head motion, which causes spurious fMRI activation. Haptic fMRI can thus reliably elicit and localize heterogeneous neural activation for different tasks in motor (movement), pre-motor (planning), and somatosensory (limb displacement) cortex, demonstrating that it is feasible to use the technique to study how the brain achieves three dimensional motor control.**

I. Introduction

Human motor neuroimaging experiments face challenging requirements: to delineate sensory and motor neural activation; identify temporal activation sequences across cortex in a closed sensory-motor loop; and guarantee the absence of spurious task-correlated fMRI activation. These challenges are further complicated by fMRI's indirect neural activation measurements—magnetic field fluctuations due to neuron-metabolism induced blood oxygenation changes [1], [2]—which require subjects to keep their head fixed during and long after performing a motor task. Subject limb motions, in addition, induce changes in the magnetic field, whose task-correlated timecourse can mimic natural neural activation [3]. Utilizing fMRI's potential for high-resolution motor neuroimaging requires noise-free protocols that maximize
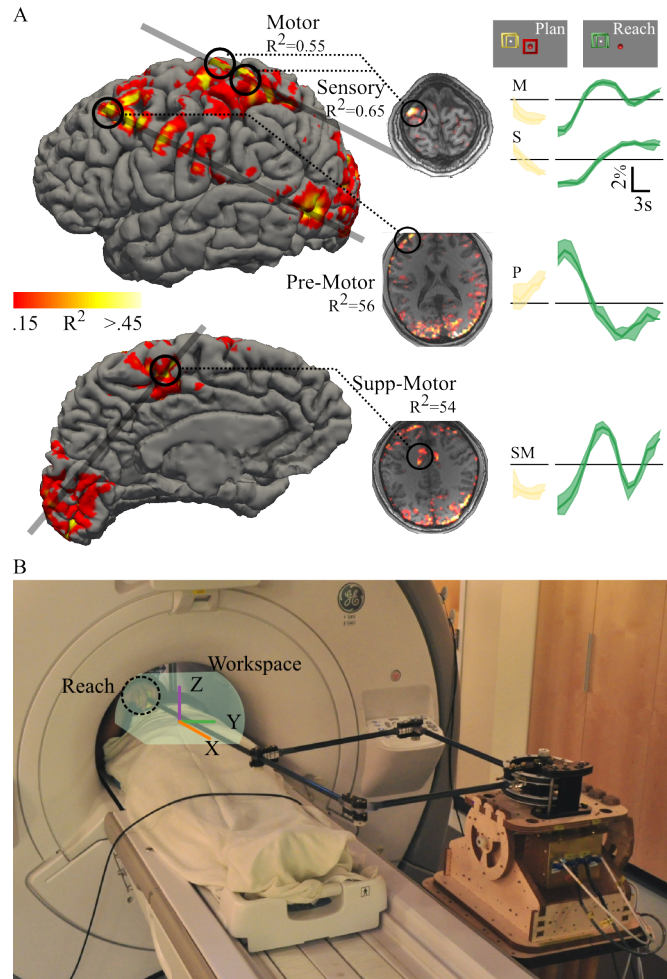

Fig. 1. Motor Neuroimaging with Haptic fMRI. A. Haptic fMRI reliably activates visual, somatosensory and motor cortex. Individual voxels in motor, supplementary motor, and somatosensory cortex activate during motion, while pre-motor cortex voxels predominantly activate during motor planning and deactivate during motion. Bootstrapped median responses are shown for exemplar voxels. B. Subjects performed these reaches in an unconstrained manner across the MRI scanner's workspace (gray highlight). Our haptic interface, HFI, tracked hand motion and a monitor (behind the scanner) provided visual feedback.

subject motion and neural activation reliability and minimize timing jitter. Ideal experiments must also be complex enough to elicit heterogeneous neural activation at a fine anatomical scale.

Combining haptics [4] with fMRI can enable high resolution experiments that study the sensory-motor system, with subjects performing complex motor tasks while haptic interfaces precisely monitor and perturb motions. To address
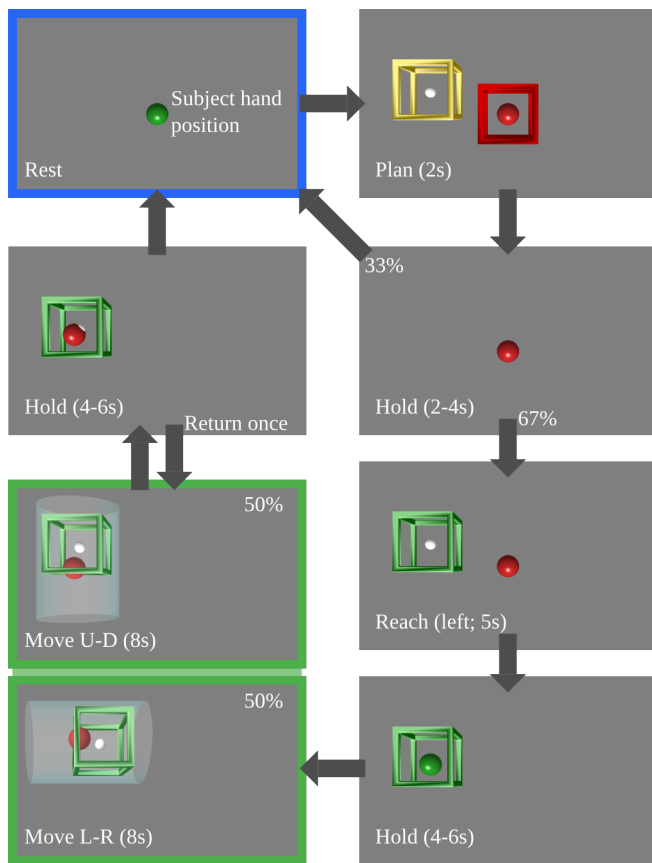
Fig. 2. A Motor Task Section. Subjects received task instructions by looking at a monitor through a mirror. Panels show the different stages of the motor task for the *left* spatial location (tasks were similar for *mid*, and *right*. Subjects started at rest (blue highlight), planned a motion to one of three spatial locations, and then either executed a reach to the location or remained at rest. The reach was followed by a hold at the spatial location, and then two iterations of a feedback control task where subjects tracked a visual sine wave trajectory by moving their hand along the y- (left-right) or z-axis (up-down). Each trajectory tracking iteration was selected at random with equal probability and followed by a static hold. Finally, subjects returned to the initial rest position. Subjects executed four such sections for each spatial position (twelve total) in each fMRI scan run, and executed 8–10 runs in a session (see Appendix for details).

motion related artifacts, past haptic neuroimaging experiments used low fMRI resolutions (voxels>27mm^3, sample time>2s) and smoothed data during post-processing [5], [6], [7], or constrained hand motions to a plane [5], [7], which limit the technique. Smoothing introduces inter-task correlations. Constrained motions can differ from natural motions [8] and can create confounding sensory neural correlates when subjects push against constraints while executing motor tasks. The primary challenge for Haptic fMRI is thus to demonstrate confound-free, reliable, and heterogeneous neural activation for complex unconstrained three degree-of-freedom motor tasks.

Here, we demonstrate that three degree-of-freedom Haptic fMRI experiments involving motor planning, reaching, and visually-guided trajectory tracking can reliably elicit heterogeneous neural activation in sensory and motor cortex. Our experiment design supports large hand motions across

the MRI scanner's workspace (>10cm) while minimizing shoulder displacement, which prevents low spatial-frequency motion induced magnetic field changes from correlating neural activation measurements across the brain [9]. As such, our protocol obtained reliable heterogeneous neural activation across cortex, even for voxels separated by a few millimeters (Fig. 1. A). Activation in pre-motor cortex during planning, and motor cortex during reaching indicates a temporal activity sequence that matches past research [10]. We calibrated our protocol (Fig. 2) to ensure reliable reaching motions, static holds, and trajectory tracking, which helped elicit similar motor statistics for four subjects across thirty-five scan runs. Finally, we found that our protocol actually helps suppress head motion during motor tasks and thus eliminates a major fMRI confound. Our results establish Haptic fMRI as the leading framework for non-invasive experiments that study how the human brain coordinates complex motions.

II. MOTOR EXPERIMENTS WITH HAPTIC fMRI

Our primary goal was to develop an experimental framework that enables neuroscientists to non-invasively study how the human brain executes complex motor tasks—in particular, tasks that are challenging or infeasible for monkeys (or any other animals) to perform and thus inaccessible using classical electrophysiology techniques. As such, we designed a protocol with multiple task conditions: motor planning, unconstrained reaching motions to a goal with no trajectory specification, precise holding motions at spatially disparate locations, and fine visually-guided trajectory tracking along two orthogonal axes (see Fig. 2). Subjects were expected to maintain the same grasp pose across the reaching trajectory and move in a reliable manner. We empirically tuned visual cue timings so subjects did not feel rushed, and did not resort to jerky motions that induce large head motions (>1mm) during either feedback control or reaching.

A. Constructing a Motor Protocol with Repeatable Sections

We strived to create an experiment protocol that can be readily integrated by existing researchers. While completely randomized tasks help keep subjects engaged, they increase the complexity of analysis code and are often incompatible with existing software pipelines [11], [12], [13]. To maximize our protocol's compatibility, we used repeatable task sections with randomized task cues. This allowed us to keep the total number of repetitions for any task condition constant over each run, making runs modular and thus replaceable. Furthermore, having sections with the same number of subject response samples makes it straightforward to cross-validate or bootstrap runs.

Each task section started at a resting state where subjects kept their right hand at a comfortable (subject-chosen) point on their abdomen. The planning cue was followed by a randomized hold, and led to a reach with a 67% chance, which kept subjects alert and avoided repetition-induced microsleep [14]. Randomizing the hold period after the reach served the same purpose. We avoided a plan stimulus for

the feedback control task, and instead focused on observing instantaneous responses to the randomly selected motion direction. Alert subjects, however, could potentially predict the task's upcoming direction near the end of some runs—if early task sections randomly selected the left-right axis more often, later sections would select the up-down with a higher probability to ensure equal trials. Task sections within a run always ended (and started) in the same rest position, but subjects could change their rest position between runs.

B. Optimizing Reach Locations

We empirically determined three reach locations that subjects could reliably access while operating HFI (Fig. 3). Our selected reach locations (left, y=-0.14m; mid, y=-0.01m; right, y=0.12m; all, z=0.035m) were easily accessible to subjects despite differences in height and physical stature (see Appendix for details). Making reach locations accessible was important to simplify the reaching motion and reduce fatigue, which helped subjects perform eight to ten runs. Each location provided enough room to support the feedback control task's displacement from the center ($\pm$3cm) along the y- and z-axis.

To determine the time available for reaching to each location, we asked subjects to execute reaches in a deliberate and reliable manner, measured the median reach initiation latency (~1s; see Fig. 4. A), and set the total time to five times that (5s). The consequent hold allowed reach related neural activation to stabilize. Randomizing the hold-state's length (4–6s) also decorrelated neural activation for reaching and the upcoming feedback control tasks, which improved our ability to statistically delineate them using a general linear model.

C. Optimizing Visual Feedback Control

We set the amplitude of the sine wave trajectory to a factor of six larger than the steady-state hand jitter during the hold period (~5mm; see Fig. 4.B). Since the reach locations were 13cm apart, the 3cm displacement of local trajectory tracking motions kept them spatially separated from each other by more than twice their peak displacement (>6cm). Randomizing the appearance of the y- and z-axis trajectories decorrelated each axis' associated neural activation from the other and also from the reach. In addition, we required executing two tracking motions (selected at random) during each motor task section because the reach-related neural activation could continue for up to 20s [2].

We optimized sine wave time periods to help subjects reliably track the visual sine wave trajectory with a root-mean-square error below a pre-decided threshold (<1cm). We found human response latency to be the limiting factor that determined how well subjects tracked the sine waves. Faster sine waves made subjects lag at the start, following which they overcompensated and rarely recovered. Humans could track sine waves with time periods of greater than six seconds, but achieving our root-mean-square error bound (median, 6–8mm; Fig. 4.C) required the time period to be at least eight seconds. Human trajectory tracking errors were
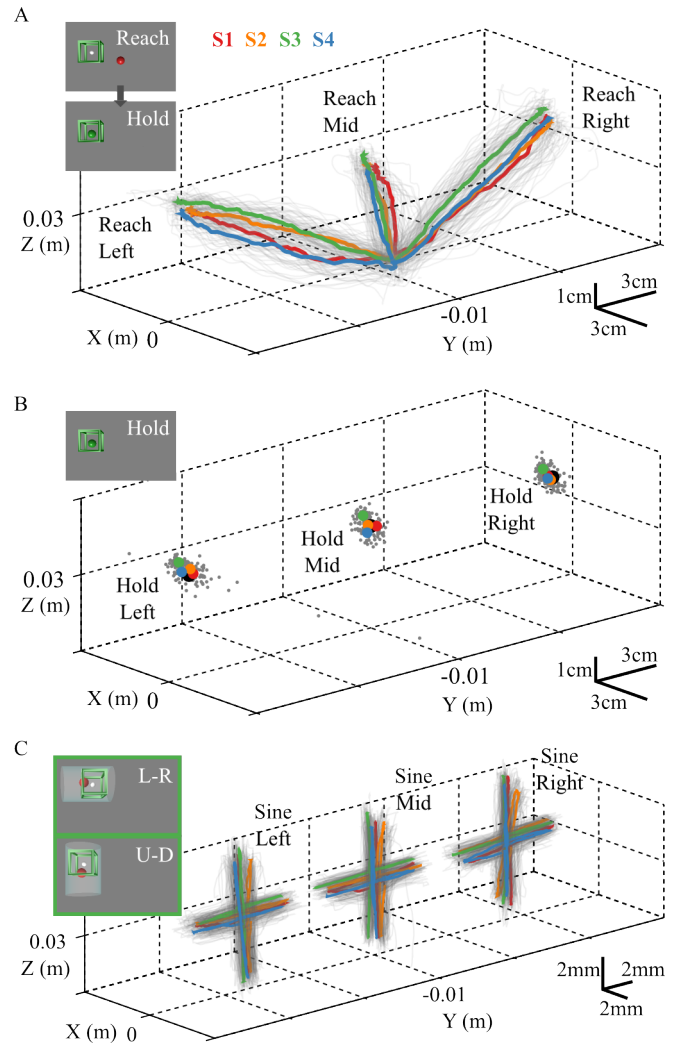

Fig. 3. Reliable Motor Trajectories. The four subjects (S1–S4) responded in a stereotypical manner to the reach, hold, and sine wave trajectory cues. A. Subjects executed reaches to the left, mid, and right locations without any spatial bias. Colors indicate medians for individual subjects. Grey indicates collated raw data. B. Subjects always moved their hand to within a few millimeters of the desired reach location, which was acceptable. Circles indicate reach-location medians for individual subjects (colors match A; black circles are desired positions). C. Sine wave trajectories tracked were also similar (colors match A). Visual cues seen by subjects during the task are inset (top-left). Subjects use HFI to control the red ball and track the white ball's motion. The controlled (red) ball turned green for position errors less than 1cm.

similar for both y- and z-axis motions, and were reliable to the point where the 95%ile median confidence interval coincides with the plotted motion lines.

III. DECORRELATING HEAD AND HAND MOTIONS

Having optimized motor task execution, our next goal was to minimize head motion and rotation along any axis to less than half the voxel width of a very high resolution fMRI scan (to avoid aliasing).

A. Head Motion Levels that Support High-Resolution fMRI

Using a 1mm³ voxel resolution—achievable with modern multi-band fMRI [15]—as a benchmark, we set our motion
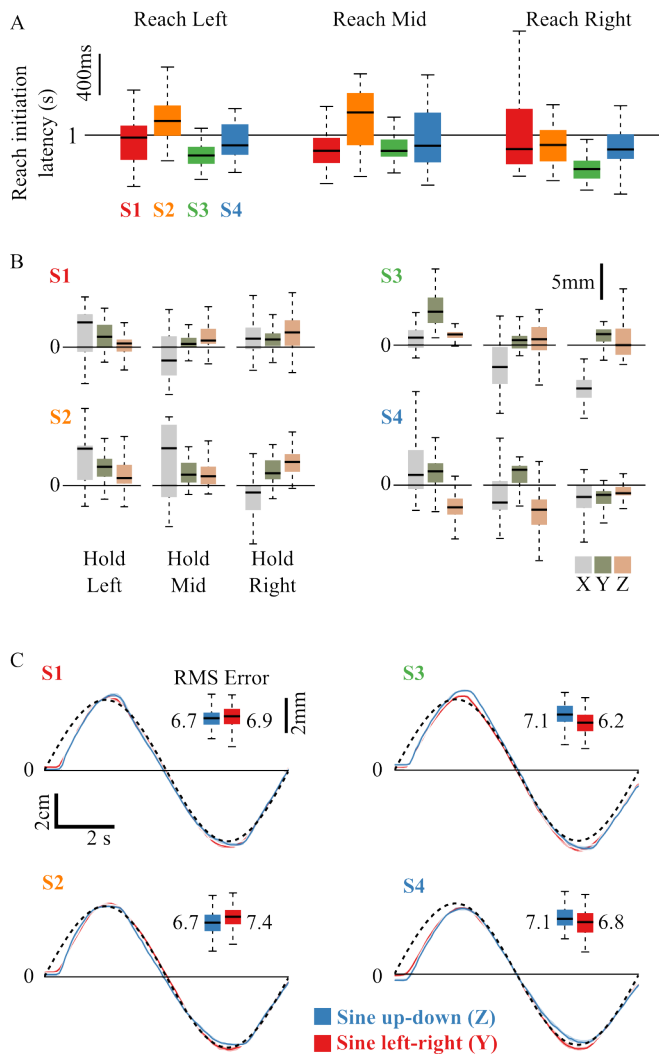
Fig. 4. Motor Trajectory Statistics. A. Response latencies for all subjects (S1–S4) were similar while reaching to the three locations. B. Subject hold positions exhibited some jitter (~5mm), which was similar across the x-, y- and z-axis. C. The root-mean-square trajectory tracking error across both axes was similar (6–8mm) across subjects. Hand motion 95%ile median confidence intervals for each axis (blue and red curves) demonstrate that subject motions were reliable (confidence intervals are small). The desired trajectory is a dashed black line. All box plots show medians, quartiles, and the inter-quartile range.
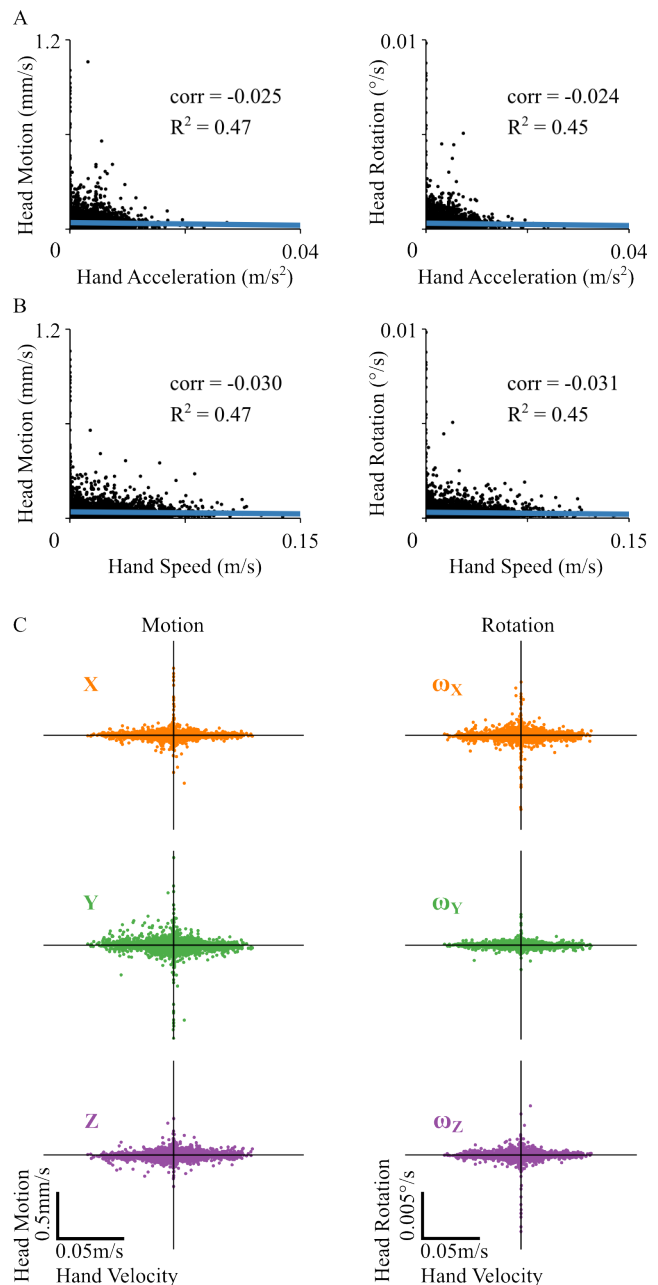

Fig. 5. Head Motion During Haptic Tasks. We compared head motions with hand speed for the four subjects' thirty-five scan runs that included four hundred and twenty task sections (see Appendix for details). A. Hand acceleration showed a weak negative correlation (-0.025) with head motion and rotation. B. A weak negative correlation was also observed for hand speed (-0.03). All the fMRI volumes during motion periods exhibited head motions below our threshold (<0.4mm/sec; $<0.005°$/sec). C. Head motion and rotation along individual axes matched the aggregate head motion trend. Each dot represents an acquired scan volume.

and rotation thresholds to <0.5mm and $<0.005°$/volume. Our efforts to optimize subject motor reliability and comfort helped achieve these head motion and rotation levels (Fig. 5). Subjects stated that using HFI actually helped them focus on the task and reduce any motion-related hand jitter, which consequently might have reduced head motion. Moreover, HFI's low and isotropic mechanical impedance (friction and inertia) [16] potentially acted as a low-pass filter for hand jitter while moving.

Even our stringent head-motion requirements, however, can induce artifacts when correlated with motor tasks. As a consequence, we also decided to test whether head motion across subjects correlated with hand motion and acceleration during motor tasks.

S1   0.08mm/s, 0.0005deg/s   S3   0.07mm/s, 0.0005deg/s

S2   0.15mm/s, 0.001deg/s   S4   0.14mm/s, 0.001deg/s

0   0.82 = fMRI Baseline   5
Noise to signal (%)
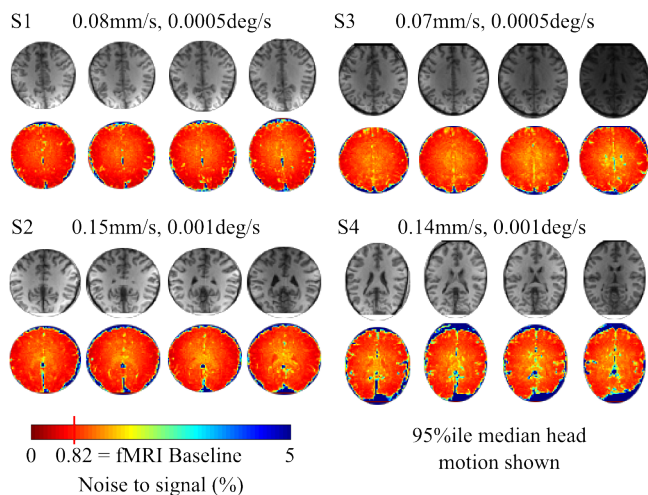
95%ile median head
motion shown

Fig. 6.   Temporal Noise Across Subjects. Low head motion levels across subjects helped minimize temporal noise during Haptic fMRI experiments. The noise distribution for each subject across cortex is similar to the scanner baseline, which demonstrates that HFI does not contribute to temporal noise. Noise was measured across 10min runs for each subject (over three different days).

B. Comparing Head Motion with Hand Speed and Acceleration

Counterintuitive to the notion that motor tasks induce head motion, we found that head and hand motions had a weak but clear negative correlation that explained a large portion of the variance (see Fig. 5. A,B). HFI's high control rate (>350Hz [16]) helped accurately estimate both hand acceleration and speed, which we compared with SPM's [11] head motion and rotation estimates. Unfortunately, head motion estimates inside the MRI scanner are limited to the fMRI volume repetition time (TR=1.57s). As a consequence, subjects might move their head and return to their original position within a scan repetition. We avoided such situations by eliminating large instantaneous hand accelerations in our protocol. All motor tasks were much longer than the TR, and accelerations were smooth. As such, the likelihood of aliased head motions having affected our results is low.

Head motion and rotation across individual axes were also uncorrelated (see Fig. 5. C), matching the aggregated statistics. Finally, all head motions and rotations that exceeded our threshold were associated with zero hand speed and acceleration. Such head motion could be attributed to breathing, swallowing, and movement of the laryngeal muscles while in the resting state.

We attribute our results to our requirement that subjects use a bite-bar and be trained to move in a fluid manner (see Appendix for details). In addition, subjects were healthy, not claustrophobic, and had been scanned for a different motor fMRI experiment in the past, all of which helped minimize head motion.

IV. Temporal Noise during Haptic fMRI

Estimating how RF noise generated by a device interferes with fMRI is complicated since the interference with sensors in the MRI machine's head coil changes for different materials. The common strategy, scanning a passive dummy object while operating the device, underestimates the noise levels because dummies are homogeneous. This enhances the ability of error-correcting field homogenization methods (*shimming*) that are built into most MRI scanners. Scanning human brains, in contrast, is realistic, but doing so overestimates noise levels because (unobserved and arbitrary) brain activity and head motion become noise covariates. To make sure our experiment protocol was robust and potentially applicable in different scanners, we required an upper bound on the RF noise in real-world conditions. As such, we tested RF noise levels directly with human subjects (Fig. 6).

V. Conclusions

Haptic fMRI overcomes limitations in classical neuroimaging experiments, whose unmonitored open-loop motor tasks [17] can not quantitatively connect neural activation to motion measurements. In this paper, we demonstrate Haptic fMRI's abilities to achieve reliable motions and neural activation given a complex motor protocol that involves three dimensional motor control. Our ability to reliably elicit heterogeneous neural activation across cortex at a millimeter scale required us to optimize our protocol and ensure stereotypical subject responses. As an interesting side-effect, we found that haptic impedance—even at our haptic interface's low levels [16]— dissipates energy and can reduce head motion. Using Haptic fMRI with our protocol promises to dramatically improve the efficacy of motor neuroimaging experiments.

While Haptic fMRI has progressed to now support high-frequency haptic rendering with all three spatial degrees-of-freedom, many engineering challenges remain. Foremost is to develop a transparent and isotropic six degree-of-freedom fMRI-compatible haptic interface that supports a multi-kilohertz control rate. Such a device's rotations will remove present grasp pose constraints on haptic experiments, and will also reduce effective inertia and friction at the end-effector (following the macro-mini concept [18]). A second goal is to demonstrate high fidelity Haptic fMRI at higher MRI field strengths and during high resolution multiplexed scanning at sub-millimeter and millisecond timescales. We expect both to be achieved in the near future.

Appendix

MRI Protocol: All fMRI scans were conducted at Stanford University's Center for Cognitive and Neurobiological Imaging on a GE Discovery MR750 3 Tesla MRI scanner, with a 32 channel Nova Medical head coil. The scan protocol was gradient echo EPI with a 16cm field of view sampled at a 64×64 resolution ($2.5 \times 2.5 \times 2.5$ mm^3 voxels), a 1.57s repetition time, a 28ms echo time, and a 72° flip angle. All scan runs were preceeded by 2nd-order polynomial shimming and were sandwiched by spiral fieldmap scans ($2.5 \times 2.5 \times 5$ mm^3 voxels). After scanning, the fMRI images were slice time corrected, motion corrected (SPM), spatially undistorted using fieldmaps, and analyzed to compute temporal noise-to-signal.

fMRI Analysis: Temporal noise-to-signal computations used the median fMRI response distribution obtained by regressing out a line from each voxels time-series, computing the absolute value of the difference between successive time points, computing the median of these absolute differences, dividing the result by the mean of the original time-series, and then multiplying by 100. R^2 values were obtained for a bootstrapped finite impulse response model using GLMdenoise [13].

Haptics motions: Subjects used HFI [16] to execute right handed motions across the MRI scanner's workspace. HFI is MRI-compatible [19] and operates without RF interference in the scanner room [16]. It has been used for Haptic fMRI scans at a higher spatial resolution than related approaches (~2x of [5], [20], and [21]). HFI's haptic control rate was 350Hz. Hand velocities were resampled to the fMRI TR using cubic spline interpolation in order to compare hand velocity with head motion.

Human Subjects: Subjects were healthy right-handed males with no history of motor disorders: S1, 19y, 170lb, 6'2"; S2, 20y, 150lb, 5'9"; S3, 29y, 185lb, 5'9"; S4, 20y, 165lb, 6'0". Informed consent was obtained in advance on a protocol approved by the Institutional Review Board (IRB) at Stanford University.

Data Collection: Each data run included twelve task sections, four each for the three different reach locations. Each section included two feedback control tasks, so each task type (y- or z-axis) was repeated four times across each spatial reach location. As such, for each spatial location, a run produced five to eight plans, four reaches, and four feedback control tasks of each type. All subjects executed one practice run inside the MRI scanner, and then executed at least eight scan runs (S1, 8; S2, 8; S3, 10; S4, 9). Each run was six hundred and thirty seconds long.

Head Motion Analysis: Subjects used a bite-bar with a custom dental dam to minimize head motion. We analyzed head motions by associating SPM's motion correction estimates with hand accelerations, speeds, and velocities measured by HFI. HFI's low position error and high control rate (0.025mm, >350Hz [16]) enabled precise measurements. We resampled the hand speeds and velocities to match motion correction estimates using cubic spline interpolation.

ACKNOWLEDGMENT

REFERENCES

[1] N. K. Logothetis and B. A. Wandell, "Interpreting the bold signal," *Annu. Rev. Physiol.*, vol. 66, pp. 735–769, 2004.

[2] N. K. Logothetis, "What we can do and what we cannot do with fmri," *Nature*, vol. 453, no. 7197, pp. 869–878, Jun 2008.

[3] J. Diedrichsen and R. Shadmehr, "Detecting and adjusting for artifacts in fMRI time series data." *NeuroImage*, vol. 27, no. 3, pp. 624–34, Sept. 2005.

[4] K. S. Hale and K. M. Stanney, "Deriving haptic design guidelines from human physiological, psychophysical, and neurological foundations," *Computer Graphics and Applications, IEEE*, vol. 24, no. 2, pp. 33 –39, March-April 2004.

[5] J. Diedrichsen, Y. Hashambhoy, T. Rane, and R. Shadmehr, "Neural correlates of reach errors," *The Journal of Neuroscience*, vol. 25, no. 43, pp. 9919–9931, 2005.

[6] R. Moser, R. Gassert, E. Burdet, L. Sache, H. R. Woodtli, J. Erni, W. Maeder, and H. Bleuler, "An mr compatible robot technology," in *Robotics and Automation, 2003. Proceedings. ICRA '03. IEEE International Conference on*, vol. 1, Sept 2003, pp. 670–675 vol.1.

[7] E. Burdet, R. Gassert, G. Gowrishankar, and H. Bleuler, "fmri compatible haptic interfaces to investigate human motor control," *Experimental Robotics IX*, vol. 21, pp. 25–34, 2006.

[8] M. Kostic, D. Popovic, and M. Popovic, "Influence of planar manipulandum to the hand trajectory during point to point movement," in *IEEE International Conference on Rehabilitation Robotics*, July 2011, pp. 1–4.

[9] T. Lemmin, G. Ganesh, R. Gassert, E. Burdet, M. Kawato, and M. Haruno, "Model-based attenuation of movement artifacts in fMRI." *Journal of neuroscience methods*, vol. 192, no. 1, pp. 58–69, Sept. 2010.

[10] D. Rosenbaum, *Human motor control*. Academic Press, 2009.

[11] K. J. Friston, J. T. Ashburner, S. J. Kiebel, T. E. Nichols, and W. D. Penny, *Statistical Parametric Mapping: The Analysis of Functional Brain Images*. Elsevier, London, 2006.

[12] "Fsl." *NeuroImage*, vol. 62, no. 2, pp. 782–90, Aug. 2012.

[13] K. Kay, A. Rokem, J. Winawer, R. Dougherty, and B. Wandell, "Glmdenoise: a fast, automated technique for denoising task-based fmri data," *Frontiers in Neuroscience*, vol. 7, no. 247, 2013.

[14] G. Poudel, R. Jones, C. Innes, R. Watts, T. L. Signal, and P. Bones, "fmri correlates of behavioural microsleeps during a continuous visuo-motor task," in *Engineering in Medicine and Biology Society, 2009. EMBC 2009. Annual International Conference of the IEEE*, Sept 2009, pp. 2919–2922.

[15] S. Moeller, E. Yacoub, C. A. Olman, E. Auerbach, J. Strupp, N. Harel, and K. Uurbil, "Multiband multislice ge-epi at 7 tesla, with 16-fold acceleration using partial parallel imaging with application to high spatial and temporal whole-brain fmri," *Magnetic Resonance in Medicine*, vol. 63, no. 5, pp. 1144–1153, 2010.

[16] S. Menon, G. Brantner, C. Aholt, K. Kay, and O. Khatib, "Haptic fMRI : Combining functional neuroimaging with haptics for studying the brain's motor control representation," in *Proceedings of the 13th Annual Conference of the IEEE Engineering in Medicine and Biology Society*, July 2013, pp. 4137–42.

[17] J. D. Meier, T. N. Aflalo, S. Kastner, and M. S. A. Graziano, "Complex organization of human primary motor cortex: A high-resolution fMRI study," *Journal of Neurophysiology*, vol. 100, pp. 1800–1812, 2008.

[18] O. Khatib, "Reduced effective inertia in macro-/mini-manipulator systems," in *The fifth international symposium on Robotics research*. MIT Press, 1991, pp. 279–284.

[19] R. Gassert, E. Burdet, and K. Chinzei, "Mri-compatible robotics," *Engineering in Medicine and Biology Magazine, IEEE*, vol. 27, no. 3, pp. 12–14, 2008.

[20] A. Hribar, B. Koritnik, and M. Munih, "Phantom haptic device upgrade for use in fmri," *Medical and Biological Engineering and Computing*, vol. 47, pp. 677–684, 2009.

[21] M. Hara, J. Duenas, T. Kober, D. Chapuis, O. Lambercy, H. Bleuler, and R. Gassert, "Design and compatibility of a high-performance actuation system for fmri-based neuroscience studies," in *Intelligent Robots and Systems (IROS), 2010 IEEE/RSJ International Conference on*, Oct 2010, pp. 2437–2442.